Research Article | Vol. 25, No. 10 | 15 May 2017 | OPTICS EXPRESS 11233

Optics EXPRESS

Carrier-envelope phase dependent photoelectron energy spectra in low intensity regime

YANG LI,[1] MIN LI,[1,*] YUEMING ZHOU,[1] XIAOMENG MA,[1] HUI XIE,[1] PENGFEI LAN,[1] AND PEIXIANG LU[1,2,3]

[1]*Wuhan National Laboratory for Optoelectronics and School of Physics, Huazhong University of Science and Technology, Wuhan 430074, China*
[2]*Laboratory of Optical Information Technology, Wuhan Institute of Technology, Wuhan 430205, China*
[3]*lupeixiang@hust.edu.cn*
**mli@hust.edu.cn*

Abstract: We study the carrier-envelope phase (CEP) dependent photoelectron energy spectra from above-threshold ionization by numerically solving the time-dependent Schrödinger equation of hydrogen atom in a few-cycle laser field at intensities in the range of (2-10) × 10^{13} W/cm^2. Depending on the electron energy and the laser intensity, the yield of the photoelectron reveals clear oscillations with respect to the CEP. At high laser intensities (larger than ~3 × 10^{13} W/cm^2), the yield of the high-energy photoelectrons (larger than $2U_p$, with U_p being the ponderomotive potential) shows two kinds of oscillations with the CEP for different electron energies. There is a clear phase jump for those two kinds of oscillations. In contrast, at low laser intensities (smaller than ~3 × 10^{13} W/cm^2), the phase of the oscillation for the high-energy photoelectron yield with the CEP is nearly independent on the electron energy, which will reduce the sensitivity of the retrieval of single-shot CEP using the method reported by T. Wittmann *et al.* [Nat. Phys. **5**, 357 (2009)] at low laser intensities. We further show that the low-energy photoelectrons display distinct CEP-dependent intercycle interference fringes, providing an alternative approach to retrieve the CEP with high sensitivity in a few-cycle laser field with low intensity.

OCIS codes: (020.4180) Multiphoton processes; (260.3230) Ionization; (270.6620) Strong-field processes.

References and links

1. F. Krausz and M. Ivanov, "Attosecond physics," Rev. Mod. Phys. **81**(1), 163–234 (2009).
2. T. Rathje, N. G. Johnson, M. Möller, F. Süßmann, D. Adolph, M. Kübel, R. Kienberger, M. F. Kling, G. G. Paulus, and A. M. Sayler, "Review of attosecond resolved measurement and control via carrier envelope phase tagging with above-threshold ionization," J. Phys. At. Mol. Opt. Phys. **45**(7), 074003 (2012).
3. D. B. Milošević, G. G. Paulus, D. Bauer, and W. Becker, "Above-threshold ionization by few-cycle pulses," J. Phys. At. Mol. Opt. Phys. **39**(14), R203–R262 (2006).
4. C. Zhai, L. He, P. Lan, X. Zhu, Y. Li, F. Wang, W. Shi, Q. Zhang, and P. Lu, "Coulomb-corrected molecular orbital tomography of nitrogen," Sci. Rep. **6**(1), 23236 (2016).
5. N. I. Shvetsov-Shilovski, E. Räsänen, G. G. Paulus, and L. B. Madsen, "Asymmetric photoelectron momentum distributions due to quantum interference in strong-field ionization by a few-cycle pulse," Phys. Rev. A **89**(4), 043431 (2014).
6. I. P. Christov, M. M. Murnane, and H. C. Kapteyn, "High-harmonic generation of attosecond pulses in the "single-cycle" regime," Phys. Rev. Lett. **78**(7), 1251–1254 (1997).
7. L. Li, X. Zhu, P. Lan, L. He, and P. Lu, "Photon channel perspective on high harmonic generation," arXiv: 1702.04084 (2017).
8. P. Agostini, F. Fabre, G. Mainfray, G. Petite, and N. K. Rahman, "Free-free transitions following six-photon ionization of xenon atoms," Phys. Rev. Lett. **42**(17), 1127–1130 (1979).
9. X. Tong, K. Hino, and N. Toshima, "Phase-dependent atomic ionization in few-cycle intense laser fields," Phys. Rev. A **74**(3), 031405 (2006).
10. G. G. Paulus, F. Lindner, H. Walther, A. Baltuška, E. Goulielmakis, M. Lezius, and F. Krausz, "Measurement of the phase of few-cycle laser pulses," Phys. Rev. Lett. **91**(25), 253004 (2003).
11. D. Milošević, G. Paulus, and W. Becker, "High-order above-threshold ionization with few-cycle pulse: a meter of the absolute phase," Opt. Express **11**(12), 1418–1429 (2003).

#290970 https://doi.org/10.1364/OE.25.011233
Journal © 2017 Received 20 Mar 2017; revised 28 Apr 2017; accepted 28 Apr 2017; published 4 May 2017

Optics EXPRESS

12. X. Liu, H. Rottke, E. Eremina, W. Sandner, E. Goulielmakis, K. O. Keeffe, M. Lezius, F. Krausz, F. Lindner, M. G. Schätzel, G. G. Paulus, and H. Walther, "Nonsequential double ionization at the single-optical-cycle limit," Phys. Rev. Lett. **93**(26), 263001 (2004).
13. B. Bergues, M. Kübel, N. G. Johnson, B. Fischer, N. Camus, K. J. Betsch, O. Herrwerth, A. Senftleben, A. M. Sayler, T. Rathje, T. Pfeifer, I. Ben-Itzhak, R. R. Jones, G. G. Paulus, F. Krausz, R. Moshammer, J. Ullrich, and M. F. Kling, "Attosecond tracing of correlated electron-emission in non-sequential double ionization," Nat. Commun. **3**(6), 813 (2012).
14. X. Ma, M. Li, Y. Zhou, and P. Lu, "Nonsequential double ionization of Xe by mid-infrared laser pulse," Opt. Quantum Electron. **49**(4), 170 (2017).
15. Y. Zhou, M. Li, Y. Li, A. Tong, Q. Li, and P. Lu, "Dissection of electron correlation in strong-field sequential double ionization using a classical model," Opt. Express **25**(7), 8450–8458 (2017).
16. A. Tong, Y. Zhou, and P. Lu, "Bifurcation of ion momentum distributions in sequential double ionization by elliptically polarized laser pulses," Opt. Quantum Electron. **49**(2), 77 (2017).
17. E. Goulielmakis, M. Schultze, M. Hofstetter, V. S. Yakovlev, J. Gagnon, M. Uiberacker, A. L. Aquila, E. M. Gullikson, D. T. Attwood, R. Kienberger, F. Krausz, and U. Kleineberg, "Single-cycle nonlinear optics," Science **320**(5883), 1614–1617 (2008).
18. X. Zhang, X. Zhu, X. Liu, D. Wang, Q. Zhang, P. Lan, and P. Lu, "Ellipticity-tunable attosecond XUV pulse generation with a rotating bichromatic circularly polarized laser field," Opt. Lett. **42**(6), 1027–1030 (2017).
19. L. Li, Z. Wang, F. Li, and H. Long, "Efficient generation of highly elliptically polarized attosecond pulses," Opt. Quantum Electron. **49**(2), 73 (2017).
20. G. G. Paulus, F. Grasbon, H. Walther, P. Villoresi, M. Nisoli, S. Stagira, E. Priori, and S. De Silvestri, "Absolute-phase phenomena in photoionization with few-cycle laser pulses," Nature **414**(6860), 182–184 (2001).
21. M. F. Kling, Ch. Siedschlag, A. J. Verhoef, J. I. Khan, M. Schultze, T. Uphues, Y. Ni, M. Uiberacker, M. Drescher, F. Krausz, and M. J. J. Vrakking, "Control of electron localization in molecular dissociation," Science **312**(5771), 246–248 (2006).
22. M. Kübel, A. S. Alnaser, B. Bergues, T. Pischke, J. Schmidt, Y. Deng, C. Jendrzejewski, J. Ullrich, G. G. Paulus, A. M. Azzeer, U. Kleineberg, R. Moshammer, and M. F. Kling, "Strong-field control of the dissociative ionization of N_2O with near-single-cycle pulses," New J. Phys. **16**(6), 065017 (2014).
23. Y. Liu, X. Liu, Y. Deng, C. Wu, H. Jiang, and Q. Gong, "Selective steering of molecular multiple dissociative channels with strong few-cycle laser pulses," Phys. Rev. Lett. **106**(7), 073004 (2011).
24. M. Kremer, B. Fischer, B. Feuerstein, V. L. B. de Jesus, V. Sharma, C. Hofrichter, A. Rudenko, U. Thumm, C. D. Schröter, R. Moshammer, and J. Ullrich, "Electron localization in molecular fragmentation of H_2 by carrier-envelope phase stabilized laser pulses," Phys. Rev. Lett. **103**(21), 213003 (2009).
25. P. B. Corkum, "Plasma perspective on strong field multiphoton ionization," Phys. Rev. Lett. **71**(13), 1994–1997 (1993).
26. G. G. Paulus, W. Nicklich, H. Xu, P. Lambropoulos, and H. Walther, "Plateau in above threshold ionization spectra," Phys. Rev. Lett. **72**(18), 2851–2854 (1994).
27. F. Lindner, M. G. Schätzel, H. Walther, A. Baltuška, E. Goulielmakis, F. Krausz, D. B. Milosević, D. Bauer, W. Becker, and G. G. Paulus, "Attosecond double-slit experiment," Phys. Rev. Lett. **95**(4), 040401 (2005).
28. T. Wittmann, B. Horvath, W. Helml, M. G. Schätzel, X. Gu, A. L. Cavalieri, G. G. Paulus, and R. Kienberger, "Single-shot carrier-envelope phase measurement of few-cycle laser pulses," Nat. Phys. **5**(5), 357–362 (2009).
29. N. G. Johnson, O. Herrwerth, A. Wirth, S. De, I. Ben-Itzhak, M. Lezius, B. Bergues, M. F. Kling, A. Senftleben, C. D. Schröter, R. Moshammer, J. Ullrich, K. J. Betsch, R. R. Jones, A. M. Sayler, T. Rathje, K. Rühle, W. Müller, and G. G. Paulus, "Single-shot carrier-envelope-phase-tagged ion-momentum imaging of nonsequential double ionization of argon in intense 4-fs laser fields," Phys. Rev. A **83**(1), 013412 (2011).
30. S. Zherebtsov, T. Fennel, J. Plenge, E. Antonsson, I. Znakovskaya, A. Wirth, O. Herrwerth, F. Süßmann, C. Peltz, I. Ahmad, S. A. Trushin, V. Pervak, S. Karsch, M. J. J. Vrakking, B. Langer, C. Graf, M. I. Stockman, F. Krausz, E. Rühl, and M. F. Kling, "Controlled near-field enhanced electron acceleration from dielectric nanospheres with intense few-cycle laser fields," Nat. Phys. **7**(8), 656–662 (2011).
31. M. Möller, A. M. Sayler, T. Rathje, M. Chini, Z. Chang, and G. G. Paulus, "Precise, real-time, single-shot carrier-envelope phase measurement in the multi-cycle regime," Appl. Phys. Lett. **99**(12), 121108 (2011).
32. A. M. Sayler, T. Rathje, W. Müller, Ch. Kürbis, K. Rühle, G. Stibenz, and G. G. Paulus, "Real-time pulse length measurement of few-cycle laser pulses using above-threshold ionization," Opt. Express **19**(5), 4464–4471 (2011).
33. D. Adolph, A. M. Sayler, T. Rathje, K. Rühle, and G. G. Paulus, "Improved carrier-envelope phase locking of intense few-cycle laser pulses using above-threshold ionization," Opt. Lett. **36**(18), 3639–3641 (2011).
34. V. Roudnev and B. D. Esry, "General theory of carrier-envelope phase effects," Phys. Rev. Lett. **99**(22), 220406 (2007).
35. T. Nakajima and S. Watanabe, "Effects of the carrier-envelope phase in the multiphoton ionization regime," Phys. Rev. Lett. **96**(21), 213001 (2006).
36. M. J. Abel, T. Pfeifer, A. Jullien, P. M. Nagel, M. J. Bell, D. M. Neumark, and S. R. Leone, "Carrier-envelope phase-dependent quantum interferences in multiphoton ionization," J. Phys. At. Mol. Opt. Phys. **42**(7), 075601 (2009).
37. F. Süßmann, S. Zherebtsov, J. Plenge, N. G. Johnson, M. Kübel, A. M. Sayler, V. Mondes, C. Graf, E. Rühl, G. G. Paulus, D. Schmischke, P. Swrschek, and M. F. Kling, "Single-shot velocity-map imaging of attosecond light-field control at kilohertz rate," Rev. Sci. Instrum. **82**(9), 093109 (2011).

Optics EXPRESS

38. Z. Wang, M. Li, Y. Zhou, Y. Li, P. Lan, and P. Lu, "Counterintuitive energy shifts in joint electron-nuclear-energy spectra of strong-field fragmentation of H_2^+," Phys. Rev. A **93**(1), 013418 (2016).
39. M. He, Y. Li, Y. Zhou, M. Li, and P. Lu, "Temporal and spatial manipulation of the recolliding wave packet in strong-field photoelectron holography," Phys. Rev. A **93**(3), 033406 (2016).
40. Z. Wang, M. Li, Y. Zhou, P. Lan, and P. Lu, "Correlated electron-nuclear dynamics in above-threshold multiphoton ionization of asymmetric molecule," Sci. Rep. **7**, 42585 (2017).
41. C. Zhai, X. Zhu, P. Lan, F. Wang, L. He, W. Shi, Y. Li, M. Li, Q. Zhang, and P. Lu, "Diffractive molecular-orbital tomography," Phys. Rev. A **95**(3), 033420 (2017).
42. M. Qin and X. Zhu, "Molecular orbital imaging for partially aligned molecules," Opt. Laser Technol. **87**, 79–86 (2017).
43. M. D. Feit, J. A. Fleck, Jr., and A. Steiger, "Solution of the Schrödinger equation by a spectral method," J. Comput. Phys. **47**(3), 412–433 (1982).
44. R. Kopold, W. Becker, and M. Kleber, "Quantum path analysis of high-order above-threshold ionization," Opt. Commun. **179**(1), 39–50 (2000).
45. B. Bergues, S. Zherebtsov, Y. Deng, X. Gu, I. Znakovskaya, R. Kienberger, F. Krausz, G. Marcus, and M. F. Kling, "Sub-cycle electron control in the photoionization of xenon using a few-cycle laser pulse in the mid-infrared," New J. Phys. **13**(6), 063010 (2011).
46. A. M. Perelomov, V. S. Popov, and M. V. Terent'ev, "Ionization of atoms in an alternating electric field," Zh. Eksp. Teor. Fiz. **50**, 1393 (1966).
47. X. Lai, W. Quan, and X. Liu, "Tunneling-induced shift of the cutoff law for high-order above-threshold ionization," Phys. Rev. A **84**(2), 025401 (2011).

1. Introduction

The advent of few-cycle laser pulses has greatly promoted the development of technologies associated with the strong-field physics and the attosecond science [1–5]. The dynamics of electron ionized from atoms or molecules by a strong few-cycle laser field critically depend not only on the amplitude and frequency of the field but also on the carrier-envelope phase (CEP). Actually, the CEP acts as a vitally important parameter for a few-cycle laser field, which determines the electron motion on a sub-femtosecond timescale and thus it has a significant effect on a number of strong-field phenomena, such as high harmonic generation (HHG) [6, 7], above-threshold ionization (ATI) [8–11], and non-sequential double ionization (NSDI) [12–16]. Nowadays, a few-cycle laser pulse with well-defined waveforms employing CEP stabilization has been widely used to generate isolated attosecond pulses [17–19], to manipulate electron emissions [20], and to control molecular dissociations [21–24].

The photoelectron energy spectrum from the ATI in a strong few-cycle laser field has been intensively studied in the past years. Generally, the relative yield of the photoelectrons from the ATI drops exponentially with increasing the electron energy. Due to the effect of electron rescattering, there is a photoelectron energy plateau ranging from ~$2U_p$ to a cutoff around $10U_p$ ($U_p = F_0^2/4\omega^2$ is the ponderomotive energy where F_0 and ω are the field amplitude and frequency, respectively. Atomic units are used unless specified otherwise) in the electron energy spectrum [25, 26]. For those high-energy photoelectrons, they are scattered backward by the parent ion so that they can gain large energy at the end of the laser pulse. In a few-cycle laser field, those high energy electrons reveal asymmetric electron emission along the laser polarization direction depending on the CEP. Thus the high-energy electrons with positive momentum and with negative momentum exhibit different energy spectra [9,20]. In the plateau region of the energy spectrum, the higher-energy electrons (near $10U_p$) are dominated by a single pair of trajectories and thus the emission direction along the laser polarization can be directly manipulated by the CEP [9, 11]. For the lower-energy electrons (near $2U_p$), more trajectories have significant contributions and a CEP-dependent attosecond double-slit interference is observed in the lower-energy region [27].

Recently, Wittmann *et al.* reported a novel measurement of single-shot CEP using the stereographic detection of the high-energy electrons from the ATI of the rare gases [28]. This stereo-ATI method measured the CEP of every single laser shot without CEP locking. In this pioneering experiment, the asymmetry parameters for the higher and lower energy electrons in the plateau region of the energy spectrum were measured and then the CEP was retrieved from the fact that the dependence of the asymmetry parameters on the CEP for the higher and lower

Optics EXPRESS

energy electrons is shifted with each other. With the two asymmetry parameters calculated from those two high-energy regions in the ATI spectrum, the unlocked CEP of every single shot was mapped on one point in a Lissajous-like parametric plot with each axis corresponding to one of the two asymmetries. Because of its convenience, this method was subsequently employed in the study of the NSDI [29] and the electron emission from the nanospheres [30]. And it was further used to retrieve the CEP of a multi-cycle pulse [31], to measure real-time pulse length [32], and to stabilize the CEP in real time [33].

Much effort to date is focused on the effect of the CEP on the photoelectrons in the high laser intensity regime while little attention is paid to the low laser intensity regime. Indeed, a few studies revealed an important role of the CEP in a few-cycle laser field with low intensity, but they mainly investigated the CEP effect on excited state populations and interference between multiphoton pathways [34–37]. Abel *et al*. experimentally studied the CEP effect on the low-energy photoelectrons at a low laser intensity of ~3×10^{13} W/cm^2 [36]. Up to now, the CEP effect on the high-energy photoelectron spectrum is rarely studied in the low laser intensity regime.

In this paper, we study the CEP-dependent asymmetry spectra and CEP-dependent photoelectron energy spectra of hydrogen atom in a few-cycle laser field from high intensity to low intensity by numerically solving the time-dependent Schrödinger equation (TDSE). Both the asymmetry parameters and the photoelectron yields reveal clear oscillations with respect to the CEP, which depend sensitively on the electron energy and the laser intensity. At high laser intensities (> 3×10^{13} W/cm^2), the yield of the high-energy photoelectrons shows two kinds of oscillations with the CEP for different electron energies. In contrast, at low laser intensities (< 3×10^{13} W/cm^2), the oscillation of the high-energy photoelectron yield with the CEP is nearly the same for different electron energies. The oscillations for the higher-energy and lower-energy photoelectrons in the plateau region show no clear phase shift, which will decrease the sensitivity of retrieving the single-shot CEP using the method reported by Wittmann *et al*. at low laser intensities [28]. We further find that the low-energy photoelectrons exhibit distinct CEP-dependent interference fringes. Based on a simple semiclassical model, we show that those fringes come from the intercycle interferences among electron wave packets emitted at time intervals separated by one laser cycle. Those CEP-dependent intercycle interference fringes might be used to retrieve the CEP in a few-cycle laser field with low intensity.

2. Theoretical methods

2.1 TDSE calculation

We first use the numerical solution of the two-dimensional TDSE to study the CEP effect on the photoelectron energy spectrum [38–42]

$$i\frac{\partial}{\partial t}\Psi(t) = H(t,\varphi)\Psi(t), \tag{1}$$

where $\Psi(t)$ is the wave function. The Hamiltonian $H(t, \varphi)$ is given by equation:

$$H(t,\varphi) = -\frac{1}{2}\nabla^2 + V(t,\varphi) + V(\mathbf{r}), \tag{2}$$

where $V(t, \varphi) = \mathbf{r} \cdot \mathbf{F}(t, \varphi)$ is the interaction of electron with the laser field, $\mathbf{r}$ is the position of the electron, and $V(\mathbf{r})$ is the Coulomb potential. The electric field of the laser pulse is

$$\mathbf{F}(t,\varphi) = F_0 f(t)\cos(\omega t + \varphi)\hat{\mathbf{e}}_x, \tag{3}$$

with φ the CEP. $f(t) = \sin^2(\pi t / mT_0)$ is the envelope of the laser pulse with m being the number of the optical cycle and T_0 being the laser cycle.

Optics EXPRESS

We use the split-operator method to solve the TDSE [43]. In order to obtain the momentum distribution, we separate the whole wave function into the inner ($0 \rightarrow R_c$) and outer ($R_c \rightarrow R_{\max}$) regions by a wave-function splitting technique [9] at any given time t_i

$$\Psi(t_i) = \Psi(t_i)\left[1 - F_s(R_c)\right] + \Psi(t_i)F_s(R_c) = \Psi_1(t_i) + \Psi_2(t_i). \tag{4}$$

Here, $F_s(R_c) = 1/(1 + e^{-(x^2+y^2-R_c)/\Delta})$ is the split function, R_c is the radius of the boundary to separate those two regions, and Δ is the width of the crossover region. Ψ_1 represents the wave function in the inner region numerically propagated under the full Hamiltonian, and Ψ_2 represents the wave function in the outer region. Because R_c is chosen large enough, the Coulomb potential is neglected and Ψ_2 propagated under the Volkov Hamiltonian analytically in the outer region. When the laser field is over, the final wave function in the outer region is the Fourier transformation of the wave function in momentum space C(p, φ, t_i)

$$\Psi_2(\infty, t_i) = \int C(\mathbf{p}, \varphi, t_i) \frac{e^{i(p_x x + p_y y)}}{2\pi} dp_x dp_y. \tag{5}$$

Here x is the direction of the laser polarization, y is the direction perpendicular to the laser polarization, and $\mathbf{p}$ is the electron momentum. Therefore, the final momentum distribution is related to the sum of the wave function in momentum space over t_i,

$$\frac{dP(\mathbf{p}, \varphi)}{dEd\theta} = \left| \sum_{t_i} C(\mathbf{p}, \varphi, t_i) \right|^2, \tag{6}$$

where E is the energy corresponding to the momentum $\mathbf{p}$, and θ is the emission angle of the photoelectron. Here we only consider the electrons emitted at exactly $\theta = 0°$ and $\theta = 180°$. The ionization probability of the electron with the positive momentum and the negative momentum are obtained from the momentum distribution at exactly $\theta = 0°$ and $\theta = 180°$, respectively,

$$P_+(E, \varphi) = \frac{dP(\mathbf{p}, \varphi)}{dEd\theta}, (\theta = 0°) \tag{7}$$

$$P_-(E, \varphi) = \frac{dP(\mathbf{p}, \varphi)}{dEd\theta}, (\theta = 180°) \tag{8}$$

where + (-) stands for the positive (negative) momentum. The asymmetry parameter $As(E, \varphi)$ is defined as

$$As(E, \varphi) = \frac{P_+(E, \varphi) - P_-(E, \varphi)}{P_+(E, \varphi) + P_-(E, \varphi)}. \tag{9}$$

The CEP-dependent asymmetry spectra and CEP-dependent photoelectron energy spectra are obtained with changing the CEP over a range from 0 to 4π with a step of 0.1π, as shown in Fig. 1 and 2 respectively. To improve the visibility, the CEP-dependent photoelectron energy spectra are normalized at the maximum for each electron energy.

2.2 Quantum-orbit theory

We also use the quantum-orbit theory [3,44] to study the CEP effect on the high-energy photoelectrons. Briefly, for the laser field given in Eq. (3), we numerically solving the saddle-point equation for the high-energy photoelectrons to obtain the dependence of the final electron energy on the ionization time. The saddle-point equations for the high-energy electrons is given by [44]

Optics EXPRESS

$$[\mathbf{k}+\mathbf{A}(t_0,\varphi)]^2=-2I_p, \tag{10}$$

$$[\mathbf{k}+\mathbf{A}(t',\varphi)]^2=[\mathbf{p}+\mathbf{A}(t',\varphi)]^2, \tag{11}$$

$$(t'-t_0)\mathbf{k}=-\int_{t_0}^{t'}d\tau\mathbf{A}(\tau,\varphi), \tag{12}$$

where I_p is the ionization potential, t_0 is the ionization time, t' is the rescattering time, and $\mathbf{k}$ is the canonical momentum before the rescattering. t_0, t' and $\mathbf{k}$ are all complex. $\mathbf{A}(t', \varphi)$ is the vector potential of the laser field at time t'. Because we only consider the electrons scattered backward, the final energy for the backward scattered electron is

$$E_{\mathrm{p}}=\frac{\mathbf{p}^2(t_0,\varphi)}{2}. \tag{13}$$

By solving the Eqs. (10)-(13), we obtain the dependence of the final energy of the backward scattered electron on the real part of the ionization time for a specific CEP value.

3. Result and discussion

Figure 1 shows the asymmetry spectra of the high-energy photoelectron ($> 2U_{\mathrm{p}}$) with respect to the CEP and the photoelectron energy at different laser intensities by solving the TDSE of hydrogen atom. The laser wavelength is 800 nm and the pulse duration is 4 optical cycles. The electron energy range shown in Fig. 1 corresponds to the plateau part in the energy spectrum. The blue color stands for photoelectrons mainly emitted with positive momentum and the red color stands for photoelectrons mainly emitted with negative momentum along the laser polarization direction.

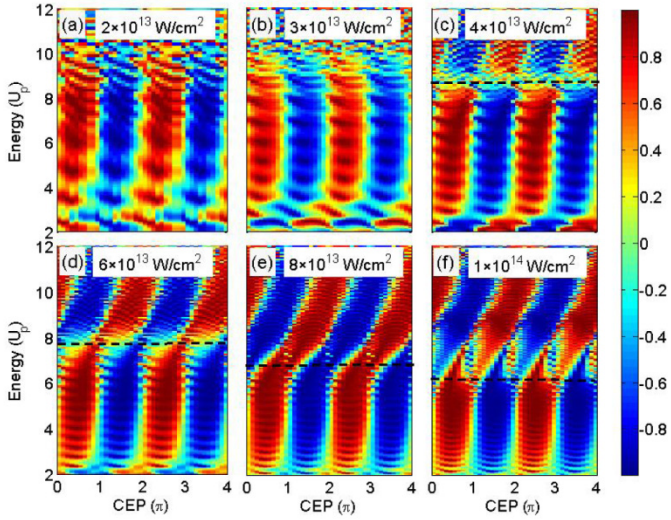

Fig. 1. The asymmetry spectra of high-energy photoelectron ($> 2U_{\mathrm{p}}$) with respect to the CEP and the photoelectron energy at different laser intensities by solving the TDSE of H. The laser pulse duration is 4 optical cycles with a wavelength of 800 nm. (a)- (f) correspond to the laser intensities of 2×10^{13} W/cm^2, 3×10^{13} W/cm^2, 4×10^{13} W/cm^2, 6×10^{13} W/cm^2, 8×10^{13} W/cm^2, 1×10^{14} W/cm^2, respectively. In (c)-(f), the black dashed lines are used to guide the boundary of the two kinds of oscillations.

One can see that the asymmetry parameter reveals obvious oscillations with respect to the CEP for the high-energy photoelectrons, and those oscillations are dependent on the laser intensity. At the highest laser intensity of 1×10^{14} W/cm^2, as shown in Fig. 1(f), one can see two

Optics EXPRESS

kinds of oscillations of the asymmetry parameter with respect to the CEP. On one hand, the oscillation in the lower-energy region of $2U_p$-$6U_p$ reveals a vertical-stripe structure. For those electrons, the oscillation of the asymmetry parameter with the CEP is nearly independent on the electron energy. On the other hand, the oscillation in the higher energy region of $6U_p$-$12U_p$ shows a tilted-stripe structure (positive slope compared with vertical stripes). With increasing the electron energy, there is a gradual phase shift in the dependence of the asymmetry on the CEP for those higher-energy electrons. The black dashed line in Fig. 1(f) is used to guide the boundary to separate those two kinds of oscillations. With decreasing the laser intensity, those two kinds of oscillations can still be distinguished from the CEP-dependent asymmetry spectra when the laser intensity is larger than 3×10^{13} W/cm^2, and the energy of the boundary obviously increases as the laser intensity decreases, i.e., the energy of the boundary is ~$7U_p$ at 8×10^{13} W/cm^2 [Fig. 1(e)], ~$8U_p$ at 6×10^{13} W/cm^2 [Fig. 1(d)], and ~$9U_p$ at 4×10^{13} W/cm^2 [Fig. 1(c)]. Interestingly, when the laser intensity is smaller than 3×10^{13} W/cm^2, the boundary disappears and only the oscillation with the vertical-stripe structure appears in the asymmetry spectra, as seen in Figs. 1(a) and 1(b). The oscillation of the asymmetry parameter with the CEP is almost independent on the electron energy at such low laser intensities. Thus, there is no clear phase shift of the oscillations with the CEP for the symmetries of the higher-energy and lower-energy electrons. As known, the method to measure the single-shot CEP in Ref [28]. relies on the obvious phase shift of the oscillations for the higher-energy electrons and lower-energy electrons in the asymmetry spectra. Therefore, the sensitivity to retrieve the single-shot CEP [28] might be reduced at low laser intensities.

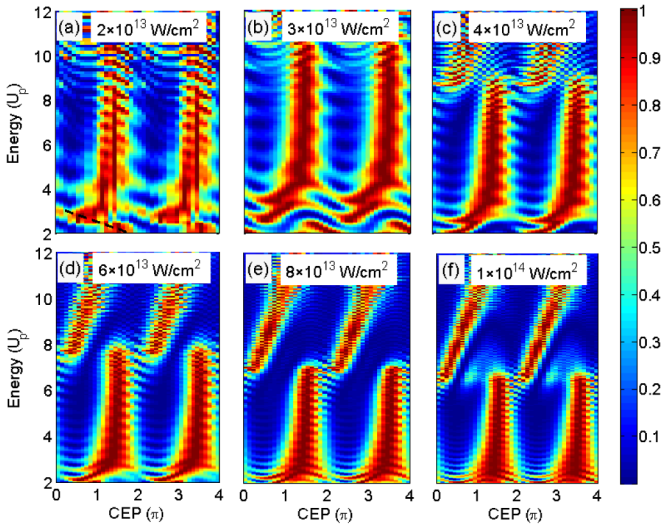

Fig. 2. The same as Fig. 1 but the color scale is the ionization probability of the electrons with positive momenta. To improve the visibility, the ionization probability is normalized at the maximum for each electron energy. In (a), the black dashed line is used to guide the intercycle interference fringe.

Because the asymmetry parameter is related to the electrons emitted along two opposite directions, i.e., the electrons with positive momenta and with negative momenta, it is instructive to analyze the CEP effect with only considering the electrons emitted along one direction. We show in Fig. 2 the CEP-dependent electron energy spectra of the electrons with only positive momenta by the TDSE calculation at different laser intensities. The laser parameters are the same as those in Fig. 1. Depending on the laser intensity, the yield of the high-energy photoelectrons also shows obvious oscillations with the CEP. At the laser intensity of 1×10^{14} W/cm^2, as shown in Fig. 2(f), two kinds of oscillations of the electron yield with the CEP can be clearly seen, i.e., a vertical-stripe structure at the energy range of $2U_p$-$6U_p$ and a

Optics EXPRESS

tilted-stripe structure at the energy range of $6U_p$-$12U_p$. With decreasing the laser intensity, the energy of the boundary to separate those two kinds of oscillations also increases when the laser intensity is larger than 3×10^{13} W/cm^2. Different with Fig. 1, there is a clear phase jump for the oscillations of the yield with the CEP at almost the energy of the boundary [45], as seen in Figs. 2(c)-2(f). This implies that the lower-energy photoelectrons might be contributed by more trajectories than the higher-energy photoelectrons [27]. When the laser intensity is smaller than 3×10^{13} W/cm^2, as seen in Figs. 2(a) and 2(b), the boundary also disappears and only the oscillation with the vertical-stripe structure is left.

In order to reveal the underlying mechanism of the above phenomena, we show the electron energy spectra with positive momenta at three laser intensities (CEP = 0.5π) by the TDSE calculation in Fig. 3(a). At the laser intensity of 1×10^{14} W/cm^2, we can see a sharp dip at the energy of ~$6U_p$. Separated by this sharp dip, two parts of electrons have significant contributions to the energy spectra. Decreasing the laser intensity to 6×10^{13} W/cm^2, the dip structure becomes less obvious. When the laser intensity is 3×10^{13} W/cm^2, the dip structure in the energy spectrum disappears and the whole energy spectrum becomes smooth except for some small peak structures.

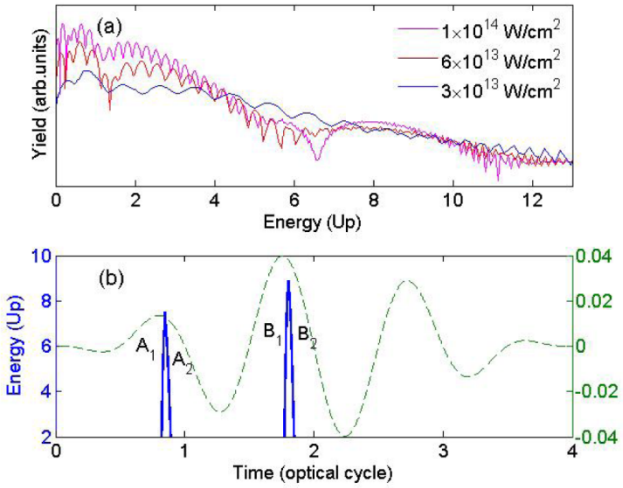

Fig. 3. (a) The electron energy spectra with positive momentum at different laser intensities. (b) The electron final energy (> $2U_p$) with positive momentum with respect to the ionization time by the quantum-orbit theory. The green curve represents the electric field with the scale given on right-side ordinate. The CEP is 0.5π and the other laser parameters are the same as Fig. 1.

The origin of those two parts of electrons at the laser intensity of 1×10^{14} W/cm^2 shown in Fig. 3(a) can be well explained by the quantum-orbit theory. Figure 3(b) shows the electron final energy with positive momentum with respect to the real part of the ionization time by the quantum-orbit theory at CEP = 0.5π. Here we only consider the electrons which scatter off the parent ion at their first return. For a specific electron energy, there are two pairs of solutions that might have significant contributions. The first pair of solutions ionized at ~$0.85T_0$ [labeled as A_1 and A_2 in Fig. 3(b)] has a lower cutoff energy of ~$7U_p$, while the second pair of solutions ionized at ~$1.8T_0$ [labeled as B_1 and B_2 in Fig. 3(b)] has a higher cutoff energy of ~$8.7U_p$. Hence, at the intensities of 6×10^{13} W/cm^2 and 1×10^{14} W/cm^2 the electrons with the energy higher than ~$7U_p$ in the ATI spectra mainly come from the solutions of the B_1 and B_2. Due to the destructive interference of the solutions of the B_1 and B_2, there will be a sharp dip at the energy of ~$6U_p$, as seen in Fig. 3(a). For the lower energy region ($2U_p < E < 7U_p$), both pairs of solutions (A_1, A_2, B_1, and B_2) have important contributions to the energy spectra. One can see a serial of peak structures separated by one photon energy in the lower-energy region of the

Optics EXPRESS

energy spectra. Those peak structures originate from the interferences among both pairs of solutions.

For the electron energy not very close to the cutoff, since the solutions of A_1 and B_1 are released near the field maximum, the relative contribution of the solutions of A_1 and B_1 is larger than that of the solutions A_2 and B_2. According to the adiabatic approximation of the Perelomov-Popov-Terent'ev tunneling theory [46], the ionization probability at a laser phase ωt of the solution B_1 can be expressed as $W \propto \exp(-\frac{2(2I_p)^{3/2}}{3|F_0\cos(\omega t)|})$ with neglecting the effect of the pulse envelope. The ratio of the ionization probability for the higher-energy electron trajectory versus the lower-energy electron trajectory for the solution B_1 is $R = W_{\text{higher}} / W_{\text{lower}} \propto \exp[-\frac{2(2I_p)^{3/2}}{3F_0}(\frac{1}{|\cos(\omega t_{\text{higher}})|} - \frac{1}{|\cos(\omega t_{\text{lower}})|})]$, where ωt_{higher} and ωt_{lower} are the tunneling phase of the higher-energy and the lower-energy electron trajectories, respectively. Since $|\cos(\omega t_{\text{higher}})| < |\cos(\omega t_{\text{lower}})|$ (as seen from the solution of the B_1 in Fig. 3(b), the relative contribution of the higher-energy electrons decreases with the decrease of the laser intensity. For each pair of trajectories, the contribution from the trajectory starting at a later time becomes negligible at low laser intensity. Thus, at the low intensities of 3×10^{13} W/cm^2, the contribution of the higher-energy electrons of the solution of the B_1 becomes negligible compared to the lower-energy electrons of the solution of the B_1. Thus, the dip structure originating from the destructive interference of the higher-energy electrons of the solutions of the B_1 and B_2 disappears. The whole energy spectrum is dominated by the lower-energy solutions of the B_1 and A_1. Those solutions of the A_1 and B_1 are extended to higher energy at lower laser intensity [47]. Thus the energy spectrum looks smooth except for the intercycle interference peaks between the solutions of the A_1 and B_1 in Fig. 3(b). As a result, only one CEP dependence of the electron yield can be observed at low laser intensities, as seen in Figs. 2(a) and 2(b).

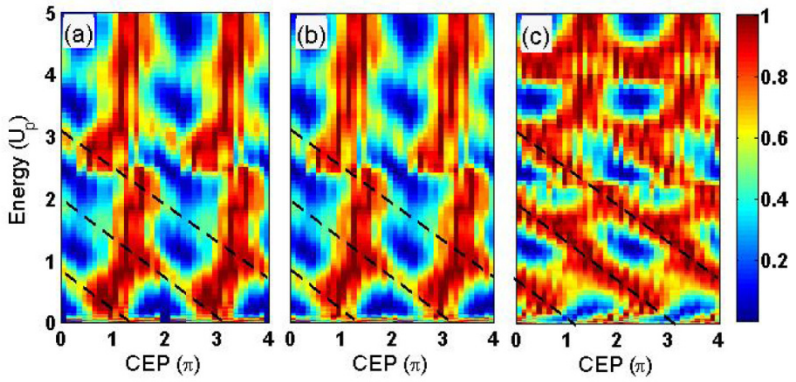

Fig. 4. The photoelectron energy spectrum (0-5U_p with positive momentum) of H at different laser pulse durations by the TDSE calculation. The laser intensity is 2×10^{13} W/cm^2 with the wavelength of 800 nm. (a)-(c) correspond to the pulse duration of 4 optical cycles, 5 optical cycles, 6 optical cycles, respectively. The black dashed lines are used to guide the intercycle interference fringes, which depend sensitively on the CEP (see text for details).

With close inspection of the CEP-dependent energy spectra at low laser intensities [Figs. 2(a) and 2(b)], we see that the intercycle interference peaks depend sensitively on the CEP, as marked by the black dashed line in Fig. 2(a). In order to see those intercycle interference structures clearer, we show the CEP-dependent energy spectra at the energy range of 0-5U_p in Fig. 4(a) with the pulse duration of 4 cycles. The CEP-dependent energy spectrum reveals an

Optics EXPRESS

interference pattern with many tilted fringes, as guided by the black dashed lines. Those interference fringes appear not only for the electrons with energy larger than $2U_p$, but also for the electrons with energy smaller than $2U_p$, which are dominated by the direct electrons. The energy spacing of those interference fringes is one photon energy, supporting that they originate from the intercycle interferences. With increasing the pulse duration, those intercycle interference fringes become more obvious, as seen in Fig. 4(b) and Fig. 4(c) with the pulse durations of five and six cycles, respectively.

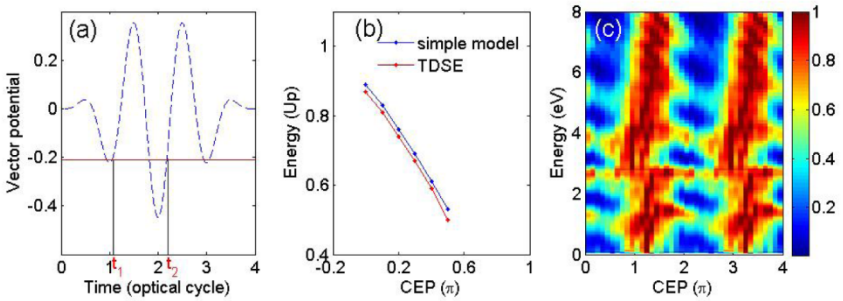

Fig. 5. (a) The vector potential of a few-cycle pulse with the pulse duration of 4 optical cycles at CEP = 0.5π. t_1 and t_2 stand for two typical ionization times with the same final momentum $p = -A(t_0)$. (b) The photoelectron energy corresponding to the interference maximum as a function of the CEP. The blue line shows the result calculated by the simple classical model and the red line shows the result calculated by the TDSE. (c) The intensity-averaged photoelectron energy spectrum with respect to the CEP of H by the TDSE calculation. The pulse duration is 4 optical cycles with the wavelength of 800 nm. The laser peak intensity is 2×10^{13} W/cm^2.

We use a semiclassical model to explain the CEP-dependence of the intercycle interference fringes. As seen in Fig. 5(a), we obtain the ionization times of two trajectories with the same final momentum from the relation of $p = -A(t_0)$ (corresponding to the same energy) at a specific CEP value. Those two ionization times are separated by almost one laser cycle, e.g., t_1 and t_2 in Fig. 5(a). The phase of the trajectory can be calculated from the classical action $S = \int_{t_0}^{\infty} (\frac{\mathbf{v}^2(t)}{2} + I_p)dt$, where $\mathbf{v}(t)$ is the electron velocity. Thus the intercycle interference fringes are determined by the phase differences of those two trajectories, i.e., $W = \cos^2(\Delta S/2)$, where ΔS is the phase difference. By scanning the electron energy, the electron energy corresponding to the interference maximum ($W = 1$) is obtained at a specific CEP. In Fig. 5(b), we show the electron final energy with respect to the CEP corresponding to the interference maximum by this simple semiclassical model. The red line in Fig. 5(b) shows the TDSE result extracted from the dashed line in Fig. 4(a). We can see that both lines show the identical slope. The result of the simple semiclassical model is in good agreement with that of the TDSE calculation. Because the phase difference between those two trajectories depends sensitively on the waveform of the few-cycle laser field, the positions of the interference maximum is determined by the CEP value. Those CEP-dependent intercycle interferences provide an alternative approach to measure the CEP at the low laser intensity with high sensitivity. With increasing the pulse duration, the intercycle inference will be enhanced and thus the interference fringes will become more obvious, as seen in Fig. 4.

To check whether the interference fringes would survive in experiment, it is important to carefully consider the intensity averaging effect in the focal volume. In Fig. 5(c), we show the intensity-averaged photoelectron energy spectra calculated by the TDSE with respect to the CEP. We calculate the CEP-dependent energy spectra for a serial of laser intensities with the peak intensity of 2×10^{13} W/cm^2. And the result of each intensity I is weighted by the volume in

Optics EXPRESS

the laser focus, i.e., $\frac{dV}{dI} \propto \frac{1}{I^{5/2}}(I_0 + 2I)(I_0 - I)^{1/2}$, where I_0 is the peak intensity. One can see that the CEP-dependent tilted intercycle interference fringes still survive after summing up photoelectron energy spectra induced by different laser intensities.

4. Conclusion

In summary, we systematically study the CEP-dependent asymmetry spectra and CEP-dependent photoelectron energy spectra of hydrogen atom in few-cycle laser fields from high intensity to low intensity by solving the TDSE. Depending on the electron energy and the laser intensity, clear oscillations are found in both the asymmetry parameter and the photoelectron yield with respect to the CEP. At high laser intensities ($> 3 \times 10^{13}$ W/cm^2), the yield of the high-energy photoelectrons shows two kinds of oscillations with the CEP for different electron energies. In contrast, at low laser intensities ($< 3 \times 10^{13}$ W/cm^2), the oscillation of the high-energy photoelectron yield with the CEP is nearly independent on the electron energy. There is no clear phase shift for the oscillations of the higher-energy and lower-energy photoelectron yield with the CEP at the low laser intensities. This implies that the sensitivity to measure the single-shot CEP will be reduced in the low laser intensity regime. We further find that the low-energy photoelectrons exhibit distinct CEP-dependent interference fringes. With a semiclassical model, we show that they come from the intercycle interferences among electron wave packets emitted at time intervals separated by one laser cycle. Those CEP-dependent intercycle interference fringes can survive with considering the intensity averaging over the focal volume, thus they might be used to retrieve the CEP in a few-cycle laser field at the low laser intensity. This work provides deep insight into the CEP effect of the perturbative fields and has implications for further efforts to study ultrafast electron dynamics in the multiphoton ionization regime.

Funding

National Natural Science Foundation of China (11674116, 61405064, 11422435, and 11234004); Fundamental Research Funds for the Central University (HUST: 2016YXMS012).

Acknowledgment

Numerical simulations presented in this paper were carried out using the High Performance Computing Center experimental testbed in SCTS/CGCL (see http://grid.hust.edu.cn/hpcc).